Appl. Magn. Reson. 16, 247–272 (1999)

Applied Magnetic Resonance

Quasioptical Hardware for a Flexible FIR-EPR Spectrometer

K. A. Earle and J. H. Freed

Baker Laboratory of Chemistry and Chemical Biology, Cornell University, Ithaca, New York, USA

Received November 17, 1998; revised March 4, 1999

Abstract. In this paper we present and summarize recent accomplishments of the Freed High Field Electron Paramagnetic Resonance group. In particular, we discuss the application of quasioptical design techniques to instrumentation problems in the far-infrared. We stress that there is no "universal spectrometer" or "universal resonator". Rather, we demonstrate with a variety of examples from the liquid and solid state that the spectrometer configuration and the resonator used should be optimized for the experiment at hand in order to achieve the ultimate in sensitivity. Quasioptical techniques and methods of analysis offer a unified framework to analyze the expected performance of a proposed spectrometer design, as well as suggest the important control parameters for optimizing the sensitivity of a given experiment as we show in the text. The flexibility of quasioptical methods will also be demonstrated with a variety of resonator designs and sample configurations.

1 Introduction

The availability of reliable, relatively inexpensive, superconducting magnets with good field homogeneity and field persistence helped to launch the development of high-field EPR more than a decade ago [1, 2]. Advances in detector and source technology have also contributed to the development of low-noise transmitters and receivers, and some of these developments are reviewed elsewhere [3]. These advances have facilitated the construction of EPR spectrometers of increasing sensitivity as improved instrumentation is incorporated into the experimental setup. Estimates of the ultimate sensitivity of an EPR spectrometer depend on the experimental conditions under which the measurements are performed. Careful estimates, correlated with experimental observations, suggest that the expected frequency dependence of the signal intensity is proportional to ω^n, where ω is the Larmor frequency, and n is an exponent that can vary from $-1/4$ to $11/4$ depending on the details of the sample size, sample losses, and resonator design [1–5].

These considerations lead us to one of the primary points of this paper that we will develop in more detail below. We emphasize that there is no "universal" EPR resonator or "universal" spectrometer that leads to the highest sensitivity for all possible experiments. For example, one may have lossy samples in some cases and very nonlossy ones in other cases. The former place greater constraints on the experimental design. Another case in point would be to perform EPR at several frequencies to, for example, study the frequency dependence of the spin relaxation. Thus, we will demonstrate how a flexible approach to spectrometer design and construction leads to useful solutions for a given experimental problem, and we will emphasize applications to samples of biological interest. As a preliminary example of design flexibility, we note that fundamental mode or slightly oversized cavities typically used at microwave or centimeter band frequencies have been used successfully up to 150 GHz [6–8] and Fabry-Pérot resonators most commonly used at FIR and higher frequencies have been used successfully down to 95 GHz [9, 10]. We have shown in the past that high-resolution EPR can be performed above 150 GHz by means of the introduction of quasioptical propagation methods [11]. Several groups besides our own are now operating EPR spectrometers based on such quasioptical design techniques. Recent developments in quasioptically based bridge designs have also led to the development of a reflection bridge in our group [12], and the techniques are becoming more common in other laboratories. Some of the more recent examples are provided by the instruments in the groups of Profs. Louis-Claude Brunel [13], David E. Budil [14], Klaus Möbius [15] and Graham Smith [16] For low-loss samples that are not size-limited, one can also work successfully in the induction mode without a resonator [16].

Thus we see that there are a number of technical solutions available for the resonant, or even nonresonant, structure used for driving the EPR resonance. However, we wish to emphasize the flexibility that arises from the use of quasioptical principles, especially given their crucial role above 150 GHz as well as their applicability even at 95 GHz. This flexibility also extends to the means by which the millimeter-wave excitation is propagated from the source to the sample, from the sample to the receiver, and how the signal is separated from the excitation (the duplexing problem). Ideally, the structures used should be sufficiently broadband that the optimum frequency, or frequencies, or field/frequency combination can be individually tailored to the experiment at hand, although, as a practical matter, one almost always works at a selection of spot frequencies across a given frequency band. The spectrometer should also be sufficiently flexible that it can operate over a range of physical parameters, e.g., temperature, a point to which we will return below. As pulse methods mature above 95 GHz, it will be important to have components that also have high-power handling capability, particularly for liquids with short transverse relaxation times (T_2). Yet, given that the available cw power at millimeter-wave frequencies above 95 GHz is at a premium, low-loss propagation is also an important consideration. This is exacerbated by the fact that propagation losses increase rapidly with frequency when conventional microwave technology is used. In order to try new experimental con-

figurations, or use the limited bore space in a superconducting magnet most efficiently; we are led to the following desiderata for the components of a high-field EPR spectrometer: (1) ease of use, (2) flexible, (3) low loss, (4) high-power handling.

We will provide examples of each of these considerations below. In particular, we hope to show the utility of quasioptical solutions [3] in developing a multipurpose, high-resolution, sensitive, high-field EPR spectrometer.

2 Quasioptical Components and EPR

If many experiments are planned, or if the instrument is part of a facility, it must be easy to use both by trained personnel and visitors to the laboratory. We require that the spectrometer consist of robust, tolerant, and easy to manipulate components. By robust, we mean that the components must be able to withstand repeated temperature cycling, frequent assembly and disassembly, for development purposes, or changing experimental configurations, as well as be insensitive as possible to inadvertent mishandling, e.g., dropping a component. By tolerant, we mean that as far as possible the components should be insensitive to misalignments induced by temperature drift or accidental mismating of component flanges. By easy to manipulate, we mean that the adjustable components should have minimal backlash and smooth mechanical operation.

Figure 1 shows a schematic diagram of our transmission-mode spectrometer, which has been a very convenient experimental configuration for us to develop most of the new techniques reported and reviewed here. The original references should be consulted for the relevant details of operation of the spectrometer for low-loss samples with a large filling factor [3]. This is an example of a novel and very useful application of simple quasioptical techniques: lens trains, horn antennas, and Fabry-Pérot resonators.

We would now like to discuss an example of how quasioptical techniques can be used to construct a resonator equipped with a goniometer. The resonator and goniometer are shown in Fig. 2, which replaces the basic Fabry-Pérot resonator shown in Fig. 1. The orientation of the polarizing magnetic field, B_0, is indicated by the arrow in Fig. 2. The orientation of the millimeter wave EPR inducing field B_1 is indicated by the arrow pointing into the page in Fig. 2. The $1/e$ diameter of the B_1 field is indicated by the dashed lines in Fig. 2, and we choose to rotate the sample S about the axis defined by support rod A in Fig. 2 in the region of highest B_1, which corresponds to the smallest $1/e$ radius. Note that the axis of rotation defined by A, B_0 and B_1 are mutually orthogonal. Given the cylindrical symmetry of the quasioptics we use to propagate the B_1 field, we may optimize the orientation of A with respect to B_1 in order to maximize the signal.

The support rod is machined from a low-loss, low-index-of-refraction thermoplastic in order to have a minimal impact on the B_1 field. We have successfully used rexolite (cross-linked polystyrene) and TPX (poly methyl pentene) for

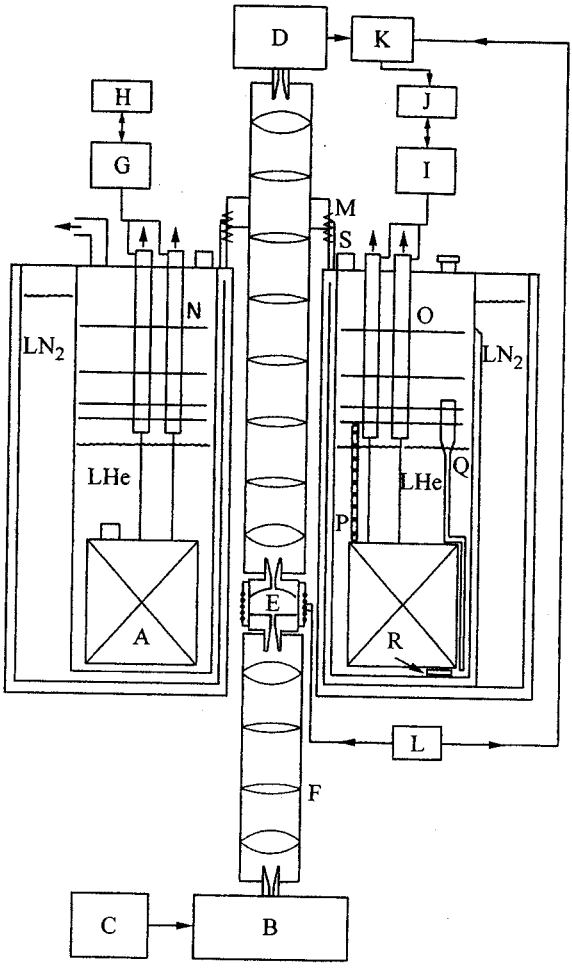

Fig. 1. Block diagram of a 1 mm EPR spectrometer. (A) 9 T superconducting solenoid and 500 G sweep coils; (B) phase-locked 250 GHz source (output power 2 mW); (C) 100 MHz reference oscillator for 250 GHz source; (D) Schottky diode detector; (E) Fabry-Pérot semiconfocal resonator and field modulation coils; (F) 250 GHz quasioptical lens train; (G) power supply for main coil (100 A); (H) current ramp control for main magnet; (I) power supply for sweep coil (50 A); (J) PC which controls field sweeps of both the main coil and the sweep coil, data acquisition, and data manipulation; (K) lock-in amplifier using DSP technology for signal amplification and detection; (L) field modulation amplifier; (M) support table for detector or InSb hot-electron bolometer; (N) vapor-cooled leads for main solenoid (nonretractable); (O) vapor-cooled leads for sweep coil (nonretractable); (P) ^{4}He bath level indicator; (Q) ^{4}He transfer tube; (R) bath temperature/bath heater resistance pod; (S) ^{4}He blow-off valves. (From [11]. The figure legend has been updated to reflect improvements to the original spectrometer.)

the support rods. Experience has shown that the rexolite support rod, although slightly more brittle than the TPX is more dimensionally stable. The rotation is accomplished by a rack and pinion drive defined by the pinion gear B and rack C. The support rod and drive train are housed in a delrin support block that is

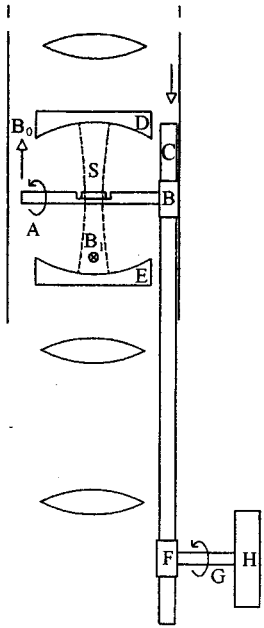

Fig. 2. Schematic diagram of a fully confocal resonator with a one-axis goniometer. (A) Sample support rod; (B) sample rotation pinion gear; (C) sample rotation rack drive; (D) upper resonator mirror; (E) lower resonator mirror; (F) rotation drive pinion gear; (G) rotation drive shaft; (H) rotation-indicating dial. In this figure, the sample is indicated by S.

not shown. The support block also contains a modulation coil in the Helmholtz configuration through which the support rod passes. The racks and pinions were chosen to have negligible magnetic impurities. In order to eliminate backlash, the rack and pinion drive is always operated in such a way that sample rotation is in the sense indicated by the arrow. In this configuration the travel of the rack is indicated by the arrow above part C. Due to the space constraints in the system, there is sufficient clearance to allow for approximately 300 degrees of rotation, which is ample for collecting rotation data in one plane. It is useful to note at this point that the diameter of our warm bore is 45 mm, which puts constraints on what can be placed in the bore.

The resonator defined by mirrors D and E is aligned by the support block. Mirror D is fixed by a double O-ring seal that has largely eliminated thermal drift in the spectrometer as discussed in more detail below. Mirror E is tunable over a limited range. The chosen resonant mode of the resonator (close to but not at the confocal separation) and the low-loss properties of the samples studied hitherto allow us to find the optimum transmitted power very quickly with minimal adjustment. In favorable cases, the loaded Q can be as high as 200 in this configuration. The rod A does cause significant scattering, however, so that the transmitted power is lower than in other resonators we have used. The reasons for avoiding the confocal separation when choosing a resonant mode are

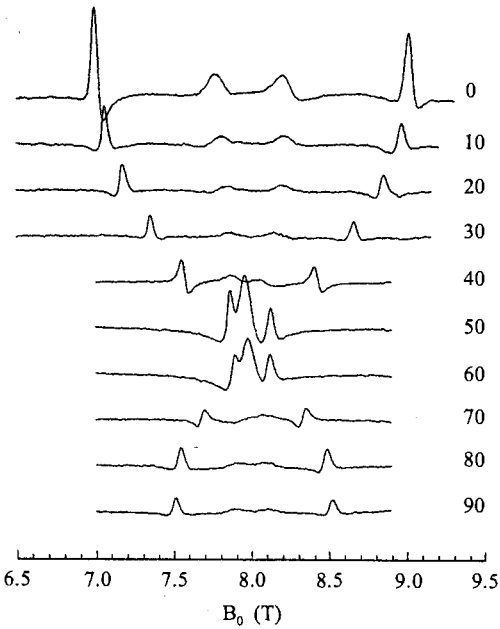

Fig. 3. A set of spectra corresponding to a crystal rotation study of Ni-doped $CdCl_6$. The orientation of the crystallographic c-axis with respect to the external magnetic field B_0 is shown to the right of the spectrum in degrees. The sample was provided by S. K. Misra. The interpretation of these spectra is given in the text.

Rotations were performed about an axis perpendicular to the crystallographic c-axis. In a coordinate system where B_0 is parallel to the z-axis, one may write down the following approximate spin Hamiltonian for the system:

$$\mathscr{H}_{\text{eff}} = g_{\text{eff}}\mu_B B_0 S_z + D'\left(S_z^2 - S(S+1)/3\right) ,$$

where $D' = D(3\cos^2\theta - 1)/2$, and $g_{\text{eff}} = (g_{\parallel}^2\cos^2\theta + g_{\perp}^2\sin^2\theta)^{1/2}$. This expression is valid in the high-field limit when one can ignore contributions from S_x and S_y. The full expression, valid at arbitrary fields, is given elsewhere [18].

One may verify by inspection of Fig. 3 that the magnitude of the values of D reported by Misra, and coworkers are correct for both sites [18]. That work reported that the narrow lines are characterized by a ZFS parameter $|D_2| = 31.12 \pm 0.150$ GHz due to Ni^{2+} ions at three magnetically equivalent sites, while the broader lines are characterized by a smaller ZFS splitting parameter $|D_2| = 6.813 \pm 0.150$ GHz due to a magnetically inequivalent site, consistent with the splittings of the observed transitions at high field. The relative intensities of the broad and narrow components are also consistent with the assignments given in that work. The high-field spectra also attest a preference for an isotropic g-value, which is within the error bounds set by Misra and coworkers [18].

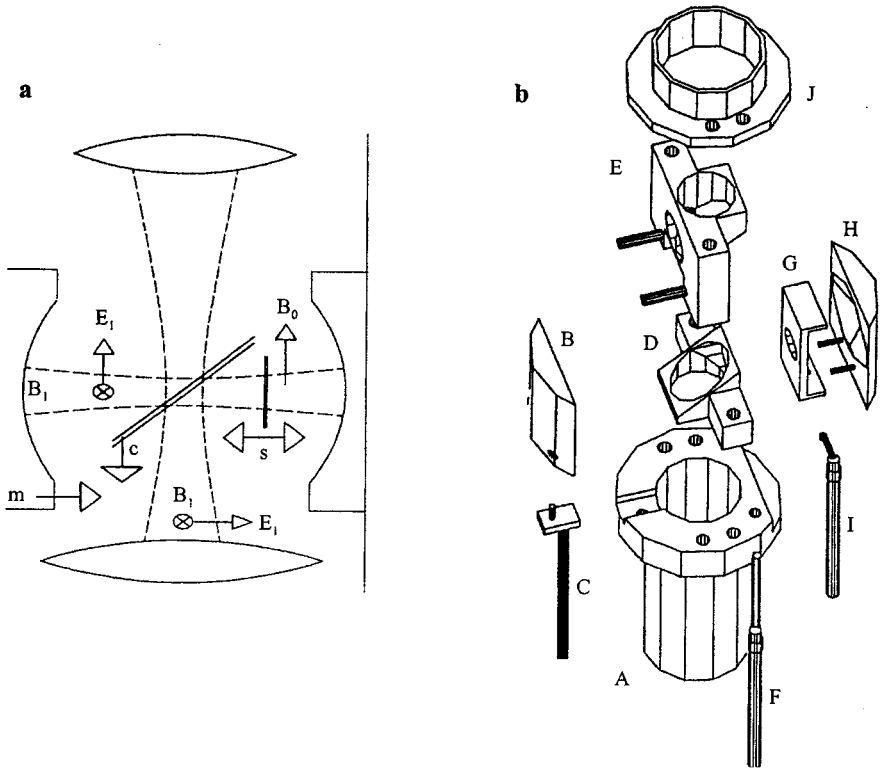

Fig. 4. **a** The relative orientations of the millimeter-wave fields in a shunt resonator. **b** Exploded view of the shunt resonator showing the tuning mechanisms in some detail. (A) Platform connected to FIR optiguide. (B) Movable shunt mirror. (C) Cam drive for the movable shunt mirror. (D) Lower section of coupling interferometer. (E) Upper section of coupling interferometer. This piece also has guide pins for movable mirror B. The dielectric sheets that define the coupling interferometer are glued to the angled surfaces of D and E. (F) A screw adjustment for the height of D. (G) Magnetic field modulation coil form and sample holder. (H) A fixed mirror with pins on which G slides. (I) The cam that moves G along the shunt resonator axis. (J) A cap to support the shunt resonator. The lenses needed to couple the Gaussian beam into and out of the shunt resonator are fixed in parts A and J. (From [20].)

It should be noted that the signal-to-noise ratio of the high-field spectra is orientation dependent. When the normal to the broad face of the sample is parallel to B_0, scattering out of the resonator is minimized and the signal-to-noise ratio is at a maximum. As the sample is rotated, however, the sample scatters more strongly and the signal-to-noise ratio is lower. Nevertheless, the signal-to-noise ratio is good enough at all orientations to allow a careful analysis of the line positions. There is also an orientation-dependent dispersion present in the spectra shown in Fig. 3. For some orientations, however, the spectra are nearly dispersion free. Methods for phasing spectra are given in several of our papers and we refer the interested reader to them for more details [19]. We intend to publish a complete analysis of the data elsewhere.

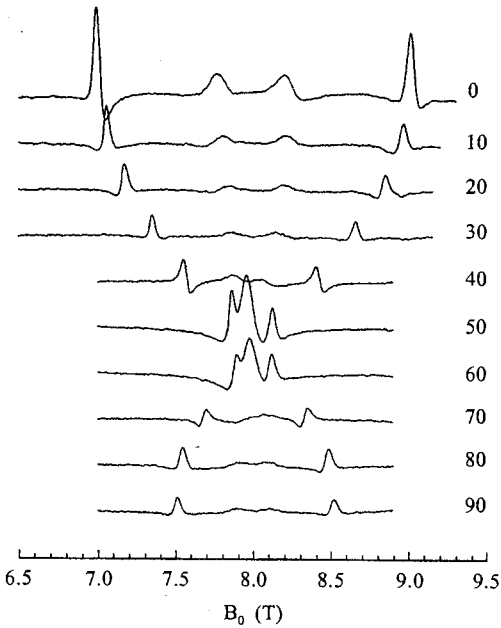

Fig. 3. A set of spectra corresponding to a crystal rotation study of Ni-doped $CdCl_6$. The orientation of the crystallographic c-axis with respect to the external magnetic field B_0 is shown to the right of the spectrum in degrees. The sample was provided by S. K. Misra. The interpretation of these spectra is given in the text.

Rotations were performed about an axis perpendicular to the crystallographic c-axis. In a coordinate system where B_0 is parallel to the z-axis, one may write down the following approximate spin Hamiltonian for the system:

$$\mathscr{H}_{\text{eff}} = g_{\text{eff}}\mu_{\text{B}}B_0S_z + D'\left(S_z^2 - S(S+1)/3\right) ,$$

where $D' = D(3\cos^2\theta - 1)/2$, and $g_{\text{eff}} = (g_{\parallel}^2\cos^2\theta + g_{\perp}^2\sin^2\theta)^{1/2}$. This expression is valid in the high-field limit when one can ignore contributions from S_x and S_y. The full expression, valid at arbitrary fields, is given elsewhere [18].

One may verify by inspection of Fig. 3 that the magnitude of the values of D reported by Misra, and coworkers are correct for both sites [18]. That work reported that the narrow lines are characterized by a ZFS parameter $|D_2| = 31.12 \pm 0.150$ GHz due to Ni^{2+} ions at three magnetically equivalent sites, while the broader lines are characterized by a smaller ZFS splitting parameter $|D_2| = 6.813 \pm 0.150$ GHz due to a magnetically inequivalent site, consistent with the splittings of the observed transitions at high field. The relative intensities of the broad and narrow components are also consistent with the assignments given in that work. The high-field spectra also attest a preference for an isotropic g-value, which is within the error bounds set by Misra and coworkers [18].

We now consider a more complicated setup that exploits the flexibility of quasioptical design for handling lossy samples. Details of the performance and operation of this device are given more fully in [20]. For our purposes, we wish to emphasize the following. The shunt resonator shown in Fig. 4 was designed to allow the collection of spectra from oriented samples characterized by a director (or principal axis of orientation), such as a liquid crystal or aligned membrane, that may be tilted with respect to the static magnetic field. Specifically, Fig. 5 shows a spectrum with a tilt of 90°. As we will show below, the enhanced orientational sensitivity at high fields merits the effort required to realize such a device.

Given that many of the samples we wish to study are lossy, which requires that the sample be in a position of small E_1 field for the millimeter waves in order to minimize dielectric losses (cf. next section), and that the field B_1 for the millimeter waves must be orthogonal to the static magnetic field B_0 in order to observe the allowed EPR transitions, there are several geometrical constraints that the shunt resonator must satisfy. The orientation and layout of the millimeter-wave fields are shown in Fig. 4a. An exploded view of the physical device that is actually used to realize these geometrical constraints is shown in Fig. 4b. The relevant physical parameters that we can vary to optimize the signal-to-noise ratio are as follows. We use an interference filter with adjustable spacing tilted at 45° with respect to the main beam and the static field B_0 to control the coupling to the shunt resonator, defined by the mirror m and the mirror opposite it in Fig. 4a. The spacing of the shunt mirrors is also adjustable. Finally, the position of the sample in the shunt resonator is adjustable. Control of these parameters is affected by control rods that drive a system of cams and shafts, as shown in detail in Fig. 4b. A thorough analysis of the shunt resonator [20] shows that control of all these parameters is necessary to optimize the signal-to-noise ratio. Examples of 0° and 90° tilt spectra of macroscopically aligned phospho-

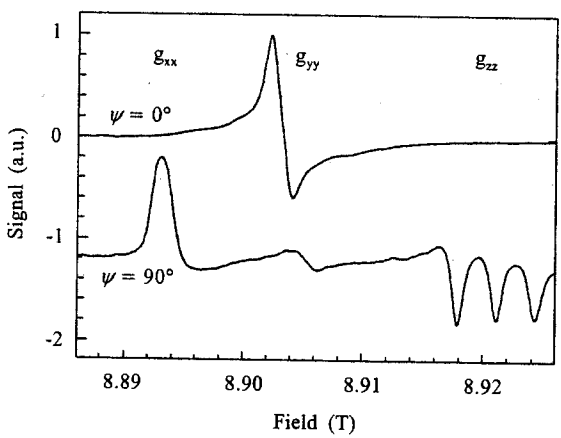

Fig. 5. Gel phase spectra of CSL in a macroscopically aligned phospholipid membrane showing the superior orientational resolution of HFEPR. (From [20].)

lipid membranes taken with this resonator and a standard resonator are shown in Fig. 5. The 0° tilt spectrum shows that the sample is characterized by strong y-ordering, where the magnetic y-axis points along the director, which is itself aligned along the magnetic field. The 90° tilt spectrum gives additional information. That spectrum shows that the ordering of the spin probe is, in fact, uniaxial because the spectral intensity is distributed nearly equally between the canonical x and z regions of the 90° tilt spectrum.

The presence of some spectral intensity at the canonical y region of the 90° tilt spectrum and of nonvanishing intensity in the canonical x and z regions of the 0° tilt spectrum indicate that the ordering is not complete and that dynamics in the system are also playing a role. It is gratifying that so much qualitative information can be read directly from the spectrum. A detailed, quantitative analysis has recently been completed on a more complicated model membrane system [21], and the reader is encouraged to consult this publication for more details. The orientational selectivity provided by the 0° and 90° tilt high-field spectra were crucial for understanding the details of ordering and dynamics in these model systems.

From an instrumentation perspective, the constraints of a narrow bore and limited clearance for control elements made the development of both the shunt cavity and the one-axis goniometer challenging. Nevertheless, the results that have been obtained with the shunt cavity [20, 21] are clear evidence of its utility, and work is under way to improve the performance and reliability of the device.

3 Flexibility

In this section, we will discuss several experimental conditions that can be varied in a flexible high-field EPR spectrometer and give some illustrative examples of the insights that can be gained from the resulting high-field EPR spectra. The ability to vary the temperature over a broad range is very useful for studying dynamic effects. Figure 6 shows spectra taken over a span of 150°C. The spectra show characteristic features of motional narrowing at the high-temperature limit and a high-field rigid-limit spectrum at the low-temperature end. Note particularly the excellent resolution of the magnetic tensor components g_{xx}, g_{yy}, g_{zz}, A_{yy}, and A_{zz}, all of which may be read directly from the spectrum at -70°C. The g_{xx} component is broadened by g-strain, which prevents one from measuring A_{xx} directly from the spectrum, although it can be found from a nonlinear least-squares fitting procedure [22]. From an instrumentation point of view, it is important to have good temperature control, especially in the presence of the large modulation amplitudes that are necessary to record the broad spectra that are in the slow-tumbling range, e.g., spectra in the middle of Fig. 6. The details of the spectral lineshape are not fit well by simple models of Brownian diffusion, even though the spin probe used, MOTA, is often treated as a Brownian particle at lower microwave frequencies. Instead, the analysis that we performed [22] on this data indicates a strong preference for a dynamic cage model, where the spin

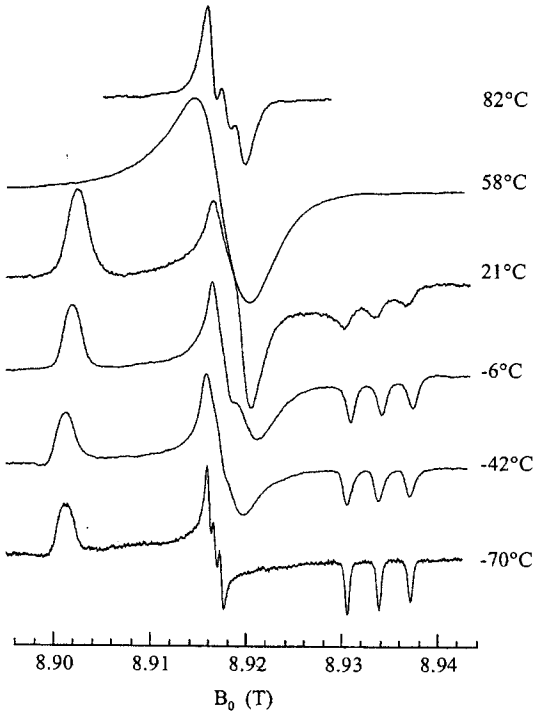

Fig. 6. Spectra of MOTA in OTP demonstrating the spectral resolution available to HFEPR from the motional narrowing limit at high temperatures to the rigid limit at low temperatures.

probe is coupled to and relaxed by the solvent cage formed by its neighbors and the solvent cage is coupled to and relaxed by the solvent degrees of freedom. This is an example of the model sensitivity that high-field spectra can provide. From an instrumentation point of view, one needs a well-calibrated magnetic field and good temperature control to profit from the enhanced sensitivity afforded by the high-field EPR spectrum.

We use a teslameter based on the NMR signal of Gd-doped D_2O to calibrate both the absolute value of the field and the sweep field of the magnet as a function of the applied current. This calibration is performed separately from spectral collection. When a spectrum is taken, the current in the magnet is continuously monitored by measuring the voltage drop across a calibrated, precision, low-impedance resistor and then converted to a magnetic field. Temperature control is done in a number of ways that relies on monitoring and adjusting the temperature of circulating gas, usually nitrogen. In this way, we can achieve temperature control to within 0.5°C from −150°C to 100°C and higher in favorable cases. For lower temperatures, we have achieved stable operation by flowing helium gas.

Given the narrow room-temperature bore of our magnet dewar and the significant cross-section of our quasioptical lens train, we are unable to use stan-

dard, commercially available, flow cryostats. We have developed and are implementing a micro-sized low-temperature insert (in conjunction with colleagues in the Cornell Low Temperature Lab) that can provide liquid-helium temperatures with a good degree of stability. This device is still undergoing development, but a brief description of the principles of operation may be of interest. We seal off a section of the warm bore with Mylar windows that are transparent to FIR radiation and evacuate the warm bore with a rotary vane mechanical pump through a liquid-nitrogen cold trap. The cryogens are transported through a thin-walled stainless-steel tube and are vented outside of the vacuum region. In addition, a proportional/integral/differential feedback system similar to existing units in the Cornell Low Temperature Lab and our laboratory with a cernox temperature-sensing element will be used to stabilize the temperature. Cernox is a registered trade mark of Lake Shore Cryotronics.

Such a low-temperature capability is important for studies of solid-state systems that relax rapidly at higher temperatures. Furthermore, there should be interesting spin physics at temperatures where $h\nu > k_B T$ such that the electron spin system is strongly polarized. Here, h is Planck's constant, ν is the Larmor frequency in inverse seconds, k_B is Boltzmann's constant, and T is the temperature. We note that 250 GHz corresponds to a temperature of 12 K.

The ability to scan broad ranges in the magnetic field is useful for those systems that have large ZFS as we have shown in Fig. 3. The value of D, the axial part of the ZFS, can be read directly from these spectra. We have shown that the rhombicity parameter $\eta = E/D$ can be determined reliably for high-field spectra using spectral simulation [23] or nonlinear least-squares fitting (S. K. Misra, pers. commun.). We have studied systems whose spectral extent is as much as 5 T at 250 GHz [23]. Such spectra extend to fields significantly higher than 9 T, beyond the operating range of our 9.4 T magnet. In practice, it is often possible to analyze partial spectra and obtain good values of the ZFS. Many of these systems have been studied at lower fields, but the simplicity of the high-field spectrum aids in the interpretation and in the extraction of the parameters from the spectral fits. This is true for the systems reported here, where the ZFS is small compared to the Zeeman interaction. It would not be true at 35 GHz or lower in frequency, and it is not a good assumption at 95 GHz. If the entire spectrum is available for analysis, the quality of the fit parameters is improved not only due to the additional information from the high-field features, but also because the experimental spectrum could be checked to ensure that it was a pure absorption spectrum. For spectra with a large, resonant paramagnetic susceptibility this is an important consideration as we have previously demonstrated [24].

Another situation where the enhanced sensitivity to the local environment at high fields translates into additional resolved structural information occurs for systems that have significant sensitivity to the local polarity. Figure 7 shows a rigid-limit lipid model membrane dispersion of sphingomyelin with 16PC spin probe. Note the resolution of the g_{xx} region into two significant populations. Previous studies [25] at 250 GHz have demonstrated the superior sensitivity of high-field EPR spectra to the polarity of local environments as reported on by the g_{xx}

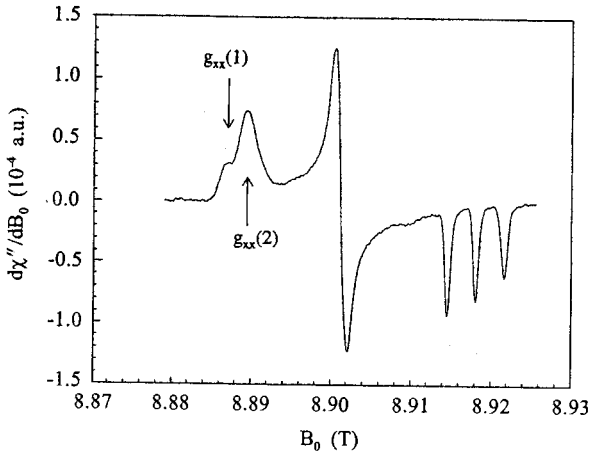

Fig. 7. Rigid-limit spectrum of 16PC spin probe in a sphingomyelin membrane dispersion. The g_{xx} region clearly demonstrates two environments, one highly polar and shifted to higher-field values corresponding to $g_{xx}(2) = 2.008582$, and one that is less polar and shifted to lower-field values corresponding to $g_{xx}(1) = 2.009152$.

component compared with lower-frequency studies. We interpret the two prominent features in the g_{xx} region as due to two sites, one characteristic of a nonpolar environment and shifted to a large g_{xx} value, $g_{xx} = 2.009152$, the other characteristic of a polar environment and shifted to smaller g_{xx} values, $g_{xx} = 2.008582$. At 9.5 GHz, aside from the collapse in resolution of this region by a factor of 250/9.5 = 26, the prominent feature at g_{xx} would be heavily overlapped in the center of the spectrum by components from the g_{yy} region of the spectrum and the $M_I = 0$ transition of the g_{zz} region for this nitroxide spin probe as we have discussed previously [25].

These particular samples present no serious experimental challenges. They have low dielectric losses because they are frozen, and the sample size is not limited by the availability of sufficient sample, hence loaded Q values of approximately 200 and filling factors near unity are achievable with these samples. Nevertheless, good temperature control and careful tuning of the Fabry-Pérot resonator are required to obtain the signal-to-noise ratio (better than 100 : 1) that we show in Fig. 7.

Although we stated that the sample size is not limited by the availability of sufficient sample and that the sample has low dielectric loss, there is still an optimum sample thickness for observing the best signal-to-noise ratio. This is because the optical, or quasioptical, properties of the sample play an important role in the sensitivity analysis of the signal, as should be expected for a sample partially filling an optical resonator.

For samples with high dielectric loss, such as aqueous samples, or samples with high conductivity, such as the electrides [24] we have studied, a different approach to resonator design is called for. In the absence of significant beam growth within

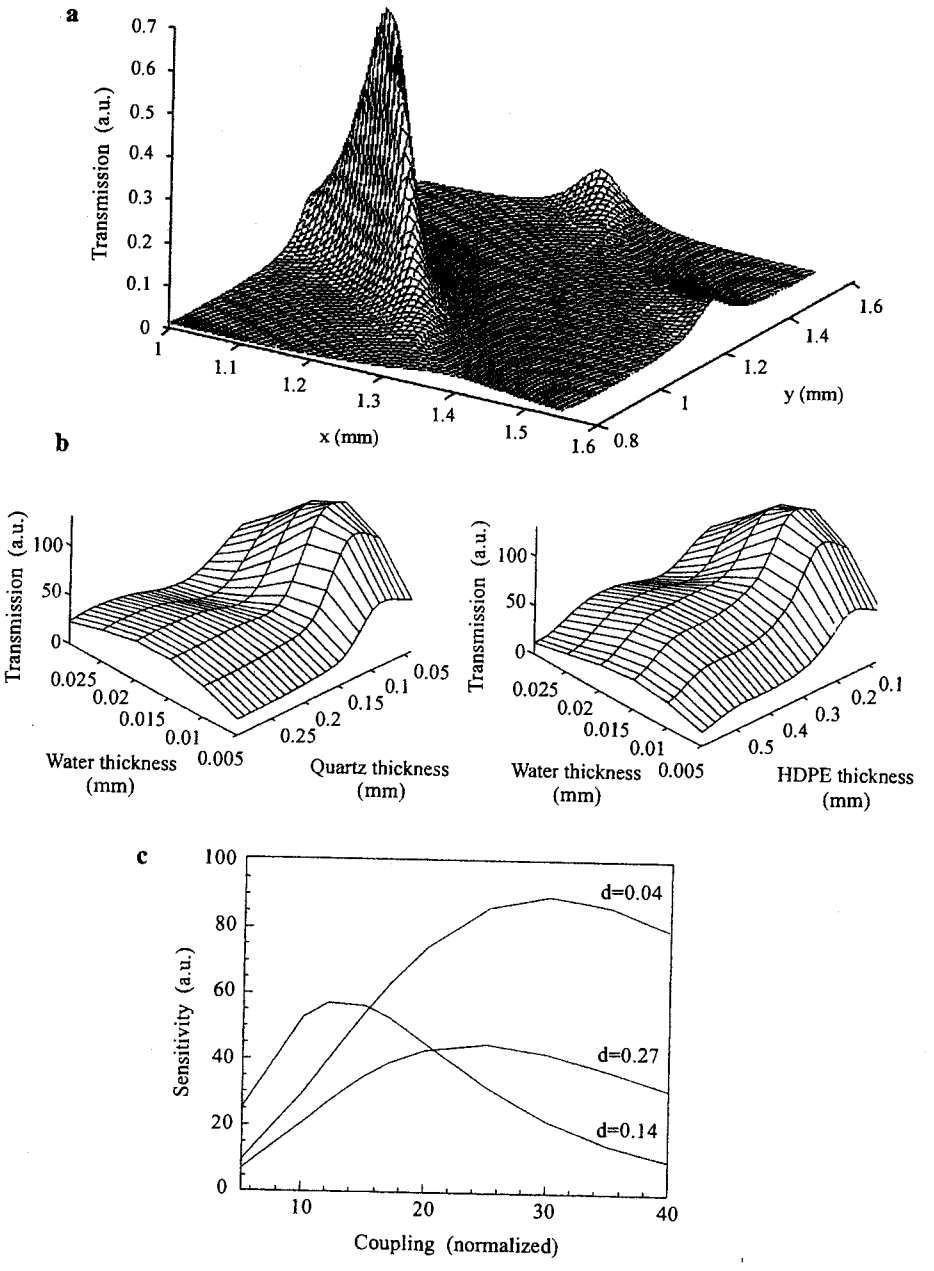

Fig. 8. **a** Theoretical transmission through an aqueous sample holder as a function of distance from mirror 1 (x) and concave mirror 2 (y). The experimental arrangement is quite similar to that shown in Fig. 2, where mirror 1 may be taken as item D, mirror 2 as item E, and the thin aqueous sample replaces the rotation support rod, item A. **b** The effect of sample thickness and the sample holder thickness for quartz and high-density polyethylene (HDPE) on the theoretical transmission through the aqueous sample holder. **c** The calculated sensitivity due to varying the cavity coupling for various thicknesses of quartz sample holders. (From [27].)

the resonator [3, 17], we can model the resonator plus sample system using well-known transmission-line concepts [17]. The details of the aqueous-sample resonator may be found elsewhere [26]. For our purposes it is sufficient to summarize a few key features that allow the aqueous-sample resonator to succeed. In our experience, the ability to vary the spacing between the mirrors and the position of the sample with respect to the mirrors is very important. We show plots in Fig. 8 of the effect of varying these parameters on the sensitivity of the sample. Furthermore, the thickness of the sample plays a very important role in the overall sensitivity, as shown in Fig. 8c. Although calculations such as these were crucial for deciding which experimental parameters it would be necessary to vary during the design and fabrication stage of the resonator development, it was only the experience gained with a number of different samples of varying water content and hence dielectric-loss properties that allowed us to develop a set of useful sample preparation guidelines at a particular frequency.

The development of a good sample holder for aqueous samples was a crucial element in our eventual success at solving this important problem. The basic requirements are that the sample holder must confine the lossy sample to a region of minimum E_1 field and be of limited axial extent. The radial extent may cover several beam waist radii, as discussed elsewhere [3, 26]. The sample-holder material should have low dielectric losses itself, and be resistant to attack by the sample. We have used Mylar and fused silica successfully. Other materials, such as PVC may also be used in some applications (D. E. Budil, pers. commun.). Any material used to hold the aqueous-sample holder together should be hydrophobic and should not interact with hydrophobic regions of the aqueous sample, such as the aliphatic chain of a lipid bilayer leaflet. We have successfully used silicon vacuum grease and paraffin to seal the edges of aqueous samples.

A careful choice of sample-holder dimensions allows us to use the same sample in our aqueous-sample resonator at 250 and 9.5 GHz. For those samples not susceptible to hysteretic effects due to temperature cycling, this is an important advantage. Figure 9 shows the signal-to-noise ratio that may be achieved with the aqueous-sample resonator for a spin-labeled protein. It was necessary to use a sensitive hot-electron bolometer (Infrared Laboratories) and repeated signal averaging to obtain this level of signal to noise. Temperature stability was also crucial for the success of this experiment. The multifrequency approach, initially demonstrated using 250 and 9.5 GHz, was shown to be effective in decomposing the complex modes of motion in a protein into its components [27]. The aqueous-sample holder and resonator were also useful in determining the field dependence of the effective g-value of Gd-chelating agents for NMR contrast enhancement agents [28]. In those experiments, the intrinsically high signal-to-noise ratio of the Gd chelates allowed us to collect single-shot spectra, i.e., no signal averaging via repeated magnetic field scans, with excellent signal-to-noise ratio [28].

During the course of the Gd chelate experiments, we found that rigidly fixing the mirror of the Fabry-Pérot resonator connected to the detector arm in our transmission-mode setup to the walls of the magnet warm bore has practically eliminated baseline drift in the spectrometer. We believe that the suppression of

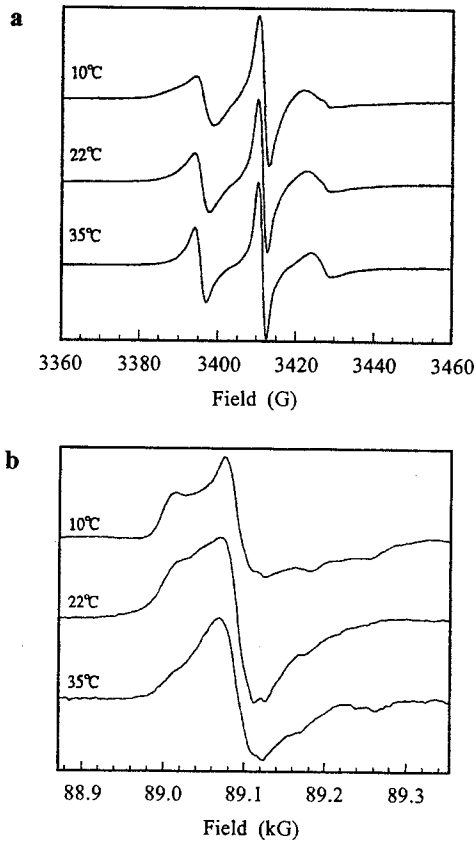

Fig. 9. **a** 9.5 GHz spectra of spin-labeled T4 lysozyme at site 69 at several temperatures of biological interest. **b** The same at 250 GHz. The increased spectral detail available at 250 GHz is evident compared to the small changes in lineshape that are discernible at 9.5 GHz. (From [29].)

the baseline drift is due to inhibiting the temperature-dependent expansion and contraction of the optical waveguide used to propagate the radiation from the Fabry-Pérot resonator to the detector. The experimental layout of the transmission-mode setup is detailed elsewhere [3]. We are incorporating this feature into our low-temperature insert design, and we expect that the additional mechanical stability afforded by this arrangement will also improve the temperature stability.

At this point, it is useful to consider the observed sensitivity for our aqueous samples. We have previously presented a detailed analysis of sensitivity for an EPR spectrometer based on quasioptical techniques [3]. It adapts the conventional analysis for microwave spectrometers [29]. In Fig. 10 we show a spectrum of oriented maleimide spin-labeled muscle fibers taken at 11°C. We estimate that there are at most $3 \cdot 10^{10}$ spins in the sample consisting of 6 muscle fibers with a radius of ca. 10 mm. The signal-to-noise ratio is estimated as 20 for this spectrum, and the linewidth of the broadest feature is taken to be 40 G. The modulation amplitude

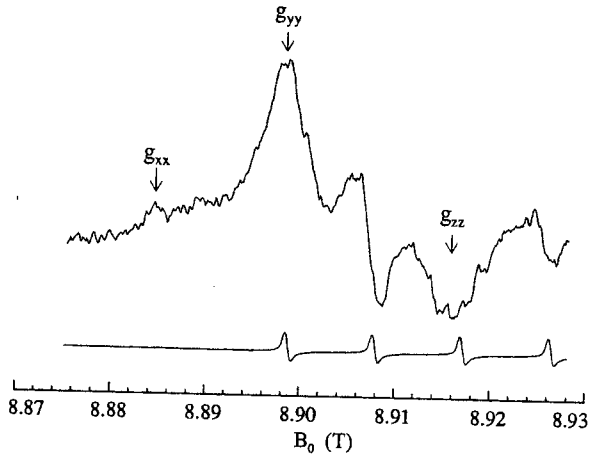

Fig. 10. 250 GHz spectrum of oriented spin-labeled muscle fiber at 10°C (upper spectrum) and a partial spectrum of Mn^{2+} in aqueous solution (bottom spectrum). The upper spectrum consists of two components. The first component is due to the spin label. The canonical turning points of the spin label spectrum are shown by arrows. The reduced intensity of the feature at g_{xx} is due to sample orientation effects. The second component is due to Mn^{2+} (with line positions as indicated by the bottom spectrum). The estimated minimum detectable number of spins is approximately $1 \cdot 10^8$ spins/G, see text for further discussion. The sample was provided by P. Fajer, and the spectra were taken by J. Barnes.

is approximately 5 G. The loaded Q of the resonator was approximately 200 and the incident power was about 2 mW. The spectrum is a composite of 10 scans where the individual scans had a time constant of 300 ms. Normalizing to a single scan, and using standard expressions to account for these factors in computing N_{min}, the minimum detectable number of spins per scan [3], we find $N_{min}M = 1.5 \cdot 10^7$ spins/G for this sample, where we have included the effect of the modulation field in the sensitivity analysis by the factor $M \equiv \Delta H_{mod}/\Delta H_{pp} = 5/40$. Here, ΔH_{mod} is the modulation amplitude, and ΔH_{pp} is the peak-to-peak linewidth of the broadest feature [3]. After inserting this value of M we have $N_{min} = 10^8$/G. This is roughly at the predicted value for N_{min} with bolometer detection [3]. It is to be compared with our previous result of $2 \cdot 10^9$ spins/G obtained in the same resonator but for a standard aqueous solution of 0.27 mM tempamine with 140 nl of sample in the active region [26]. The much smaller muscle-fiber sample (estimated volume of 10 nl) may well be interfering less with the quasioptical properties of the Fabry-Pérot resonator providing better signal-to-noise ratio [26]. In addition, a number of minor improvements to the resonator and spectrometer performance likely accounts for some of the improved signal-to-noise ratio. The main point is that very small samples with a limited number of spins can be detected.

4 Low Loss

So far in our detailed discussions, we have limited ourselves to the influence of the performance of the resonator on the ability to observe good signal-to-noise ratio

from a sample. As we discussed in the previous section, however, the resonator is connected to a transmission line that must propagate the radiation from the source to the resonator and on to the detector. Let us now examine some of the characteristics of various transmission lines used in high-field EPR spectrometers.

One common technique is to use waveguide or oversized waveguide to propagate the radiation over the required distances [9]. A disadvantage of this approach is that overdoing can occur if special care is not taken at waveguide bends and other discontinuities. Fundamental mode waveguide is also extremely lossy at frequencies above 95 GHz and the losses and sensitivity to waveguide imperfections just get worse as the frequency increases.

Another approach, and the one that we advocate at 95 GHz and higher, is to use quasioptical propagation techniques. These techniques are reviewed with specific application to EPR elsewhere [3]. A more general overview of quasioptical techniques as a systems approach is also available [17]. Basically, the quasioptical approach uses the paraxial approximation and physical optics to derive a set of approximate equations that can be used with confidence within stated ranges of parameters for designing and predicting the performance of mirrors and lenses (and resonators). Within the stated limits, it is no more difficult to use the quasioptical approach than it is to use geometrical optics to design a simple optical system.

Thus, the quasioptical approach is a free-space propagation technique with the corrections to ray optics due to diffraction included in a consistent, analytically tractable way. Given that the conductivity of the most commonly used metals, such as aluminum, brass, copper, silver and gold, for quasioptical components is quite high from 95 GHz up to 1 THz, it is possible to design and build reflecting optics with nearly ideal performance. We should note that most reflecting optics are used off-axis, i.e., in a nonaxisymmetric way, which can introduce significant aberrations. However, careful design of the mirrors and their separation can be used to minimize the effect of these aberrations. With care, mode conversion and beam distortion amplitudes can be kept below 1%, which is on a par with the performance of grid polarizers as we discuss below. Several examples relevant to EPR have been discussed in the literature [12, 16] and the methods of quasioptical analysis have been used to evaluate their performance [3].

Quasioptical techniques are also useful for designing and evaluating the performance of reflection-mode systems. We summarize a few advantages of the reflection mode of detection here. The references should be consulted for more details [3, 12, 16]. The first advantage we note for a spectrometer based on a reflection scheme is that it is possible to detect a small signal on a small background. In the transmission mode, even if the resonator is optimally coupled to the transmission line, 1/4 of the available power from the source is incident along with the signal, and this can reduce the sensitivity of the detector. Another problem is that the dynamic range of the detector may not be sufficient to cleanly separate the signal from the background power [3]. For a reflection-mode spectrometer, if the resonator is critically coupled to the transmission line, then there is no reflected power except that due to the EPR signal. Thus we avoid detec-

tor saturation problems and dynamic range issues. Due to scattering losses in our iris-coupled transmission-mode resonator, the background power incident on our detector, e.g., Schottky diode or InSb hot-electron bolometer is not the 1/4 of the available power of the source one would estimate for an optimally coupled resonator. The insertion loss is more nearly 20 dB instead of the optimum value of 6 dB. Nevertheless, the background power we observe is somewhat higher than optimum for the InSb hot-electron bolometer.

One could use an rf bucking scheme with the transmission-mode system to ameliorate the background power problem by injecting a wave in anti-phase with the background transmitted power, but the implementation would be tricky because of the inherently long path lengths involved. Another alternative to a straight transmission-mode resonator is to operate in the induction mode, i.e., excite the EPR line in one polarization state and observe in the orthogonal polarization state. This was done at 140 GHz in a pulsed configuration [8]. However, induction-mode operation can more easily be implemented in a reflection-mode configuration [16]. Moreover, the reflection mode of operation is intrinsically more compact than the transmission mode of operation. Finally, it is a more flexible mode of operation, since all of the relevant quasioptical elements are close to one another on an optical breadboard [12, 16].

We show schematic diagrams of two possible modes of operation using a reflection bridge in Fig. 11. Both rely on quasioptical methods to separate the EPR signal from the excitation. In particular, the technique of polarization coding is used for signal discrimination. The scheme shown in Fig. 11a, which is a quasi-optical analogue of a microwave bridge with a circulator, has been implemented at Cornell [12]. Its sensitivity operating at 170 GHz was a factor of three better than the transmission-mode spectrometer operating at 250 GHz [12]. When corrected to a common frequency, the estimated improvement was a factor of 7.5 [12]. The scheme shown in Fig. 11b is an example of a quasioptical induction-mode spectrometer. In this scheme, the sample's rf susceptibility tensor generates a cross-polarized response that is many dB down from the rf excitation and is thus ideally suited for detectors that saturate easily. Reference [16] should be consulted for more details. The success of these techniques depends on polarizers with good isolation between the co- and cross-polarized components of the beam. Based on our own measurements and the estimates of others [17], we believe that polarization isolation at the level of 30 dB is a good engineering estimate, a point to which we return below.

We should note that the design of refracting optics for quasioptical systems is a bit more challenging, especially if there are a large number of surfaces, because of reflections from the dielectric discontinuity at the lens surface. Satisfactory solutions for systems that span only a narrow frequency band exist and are detailed elsewhere [3, 17]. We have used reflecting and refracting optics successfully in our spectrometers.

One of the features of the quasioptical approach is that the transverse extent of the beam must be sufficiently large that diffraction is kept within reasonable bounds. As the frequency becomes lower, this is more of a constraint, particu-

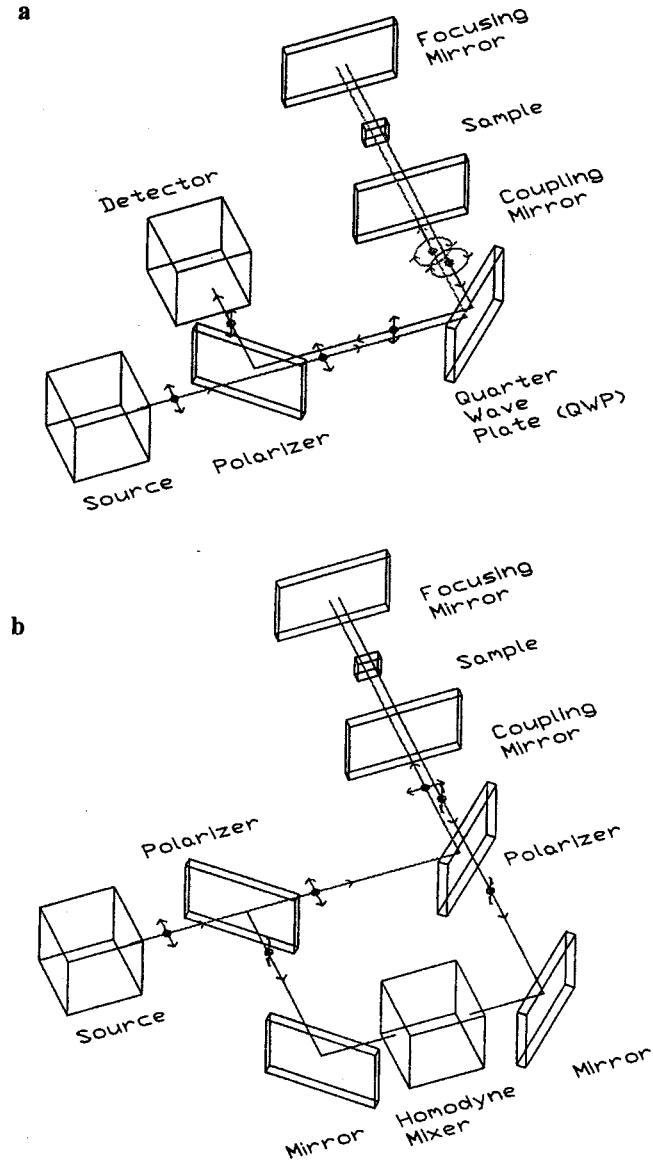

Fig. 11. **a** A schematic diagram of the reflection bridge discussed in more detail in [12]. The quarter wave plate (QWP) converts horizontally polarized radiation from the source into circularly polarized radiation, which irradiates the spins. The coupling mirror and focusing mirror define the Fabry-Pérot resonator used to enhance the B_1 field at the sample. The signal from the resonator, which is circularly polarized in the opposite sense, is converted by the QWP into vertical polarization, causing it to be reflected by the polarizer, directing it to the detector. **b** A schematic diagram of an induction-mode reflection bridge with an LO bias arm along the lines discussed in [16]. Here the horizontally polarized radiation from the source is used to irradiate the spins in the resonator. However, only the vertical component of the signal passes through a polarizer and into the detector operated as a homodyne mixer.

larly if we must propagate the radiation in a region of limited radial extent, such as the warm bore of a superconducting magnet. We have used lenses in the past to overcome this problem, but as we have already noted, lenses are only useful for narrow-band applications.

For these reasons, we prefer to use corrugated waveguide, which is a class of HE_{11} guide that propagates a so-called balanced hybrid mode with very low loss and a very high degree of polarization purity. A detailed description of corrugated waveguide may be found elsewhere [30]. It has losses which scale as $1/a^3$ where a is the minor radius of the corrugations. Losses as low as 0.01 dB/m or even lower can be achieved with corrugated waveguide [30]. The corrugations make the walls of the waveguide reactive and thus suppress wall currents which in turn limits the losses to the exceptionally low levels reported in the literature. We note that low-loss, broadband miter joints are available for corrugated waveguide if it is necessary to guide an HE_{11} beam around a tight corner [31].

Doane's review article [30] should be consulted for more details. It should be noted that there are higher pass bands for corrugated waveguide, above the first Bragg reflection peak, characterized by higher ripple and greater sensitivity to wall imperfections [32]. For some applications, however, this may still be a viable mode of use, although the performance is not as good as in the design passband [32]. These techniques easily allow bandwidths of 2 : 1 or higher [30–32].

We have used electroformed copper in the past for our corrugated waveguide. However, for variable-temperature experiments, the heat capacity of the copper introduces a significant heat load. Current designs favor the use of german silver, which has a nice balance of machinability and low heat conductivity, combined with good conductivity for low-loss operation.

Another important consideration for low-loss performance is the processing efficiency of the optical system. The quasioptics formalism allows us to evaluate the polarization purity of the Gaussian beam as it passes through the system as well as scattering to higher-order modes, which can be treated as a loss mechanism, and scattering from finite apertures. For some applications, the polarization purity is not a concern. Given that the polarization of the beam is available for coding information, it is often worthwhile to exploit this flexibility to maximize the duplexing efficiency of a reflection bridge. At higher frequencies, where power is at a premium, minimizing the losses in the system is an extremely important consideration in the design and performance of the system. These considerations are discussed more fully in [3, 12, 16, 17].

5 High-Power Handling

Low-loss modes of operation are even more important for those systems that utilize high-power sources, such as the pulsed spectrometer at 95 GHz currently under development in our laboratory for studies of relaxation in liquids. In order to protect delicate receivers and other sensitive components in the system it is necessary to reduce pulse feedthrough and other "stray" rf fields in the bridge. Based on our discussion of the polarization isolation performance we have given

above, we believe it is possible to design for pulse feedthrough isolation at the 30 dB level [3, 12, 17]. Receiver protection can also be implemented using quasioptical delay lines and PIN protection switches at the receiver input, so that the receiver is only on when the EPR signal is present.

Another advantage of quasioptical components is that wall currents in HE_{11} guide and the scalar horns that are used to launch Gaussian beams are intrinsically at very low levels. This means that dissipation in those sections of the optical train that are confined to HE_{11} guide is very low, and thus their power handling capability is naturally much higher than conventional waveguide. In fact HE_{11} guide is often used to form the resonant cavity in FIR lasers [32]. Other quasioptical components such as mirrors and wire grid polarizers can dissipate Joule heating readily because of their relatively massive construction. If necessary these components and others, such as scalar feed horns, may be mounted on heat sinks without compromising their performance.

6 Fabrication of Components

Quasioptical components are diffraction-limited in terms of their optical performance [17], and thus the surfaces of conic section mirrors and other reflecting surfaces must be held to strict tolerances in order to achieve maximum performance. Given that the relevant wavelengths are on the order of millimeters, however, surface tolerances of tenths of a millimeter will in fact give diffraction-limited performance over much of the near-millimeter band. Such tolerances are standard workshop tolerances, so that fabrication of, e.g., conic-section mirrors need not be given over to optical houses. Some papers that discuss standard machine shop procedures for fabricating off-axis conic-section mirrors are given in [33–35].

The production of wire grid polarizers typically requires fine tungsten wires for strength. They may be wound in pairs on a standard coil winder [36], although higher yields are obtained if the winding speed can be made to accommodate the variable tension on the tungsten wire as the polarizer frame rotates (R. Wylde, pers. commun.). Cross-polarization levels of 30 dB or better are typically achievable [17].

Concave on-axis mirrors, suitable for use in Fabry-Pérot resonators may be made by depositing a layer of metal, either by chemical means, or by sputtering, on a plano-concave lens of the appropriate radius of curvature. In order to have a highly reflecting surface, it is necessary to have a film thickness of several skin depths. At 95 GHz, a thickness of 1 mm suffices for a high-reflectivity surface. The relevant formulas are given in [17].

In many applications of high-field EPR, it is necessary to have oscillating fields at other frequencies besides the millimeter wave frequency. For cw EPR, an example of such a field would be the magnetic field modulation. ENDOR and Triple are other applications where there is an additional oscillating field or fields [37]. In such circumstances, it is quite useful to minimize the amount of

metal that is in contact with the oscillating fields, as the Lorentz forces due to the oscillating fields can be quite severe at high fields. Eddy current heating can also be a significant problem if care is not taken to minimize its effect. We have found that it is possible to generate 50 G modulation amplitudes in the 250 GHz transmission mode spectrometer. However, when we tried to use it on an inorganic Ni(II) sample (ca. 0.5 cm^3 volume) there was considerable heating of the sample, which destroyed it.

Such high modulation amplitudes are justified for the very broad resonance lines that can occur in transition metal ion powders at high fields. For low-loss samples the modulation-amplitude limitation can be overcome in favorable cases by working at lower modulation amplitudes than would be optimum (modulation amplitude $\ll$ linewidth/10) and increasing the sample size. Reducing the modulation frequency is occasionally an option as well, although the signal-to-noise ratio as a function of modulation frequency should be carefully evaluated for a given experimental configuration. The type of detector chosen can have a significant influence on the optimum modulation frequency [17, 29], (M. Nilges, pers. commun.). For some samples, where the ratio of the linewidth ΔH_{pp} to the achievable modulation amplitude ΔH_{mod} is several orders of magnitude greater than unity, it can be desirable to dispense with magnetic field modulation entirely and detect the absorption directly (N. Dalal, pers. commun.), although the signal-to-noise enhancement afforded by magnetic field modulation is a powerful argument in its favor whenever it is practical.

7 Modular Bridge Design

One of the great advantages of quasioptical components is that the optical circuit one constructs has a high degree of flexibility in the size of the components that one uses. Thus, if one must propagate a beam over distances characterized by meters, and truncation is not a problem, then one may choose large aperture optics and a large beam waist to minimize diffractive-beam growth and maximize the distance over which a collimated beam may travel with negligible loss. If the available aperture is limited and a small level of loss may be tolerated, HE_{11} guide, in one of the forms discussed above is a suitable choice. For space-qualified missions where space and payload are at a premium, compact structures may be designed and built as discussed elsewhere [17]. The disadvantage is that there are no standard components for a given frequency, or frequency band, requiring that the spectroscopist design each system de novo or have a more experienced instrumentation specialist do the design and fabrication. As more and more quasioptical EPR spectrometers are built, the advantages of the modular approach to quasioptical component design and fabrication based on the half cube technology are becoming increasingly apparent [16, 17, 38], (M. Nilges, pers. commun.).

From these examples, it is clear that the quasioptical approach is a flexible one. The constraints provided by the particular application at hand are often useful

for making a rational choice between various possible design solutions. If broadband frequency performance is desired, then it is possible to utilize the principle of the Gaussian beam telescope to have frequency-independent performance over an octave in frequency [12] or more in favorable cases [17]. If operation at a single frequency is desired, then all of one's efforts may be directed towards optimizing performance within a narrow bandwidth.

Thus, one may choose a particular component layout that corresponds, e.g., to a given, optimum level of cross-polarization performance in a reflection bridge for a fixed frequency. In a broadband system, different choices would be necessary to ensure that the cross-polarization isolation was acceptable over the entire band. Different design choices would again be relevant if operation at spot frequencies in a given band were desired. From the design perspective, the formalism used to analyze quasioptical systems performance is flexible enough to deal with all of these situations, which is a considerable advantage when a number of competing criteria and constraints are at hand. In addition, the availability of powerful polarization coding techniques allows the spectroscopist to efficiently detect and manipulate the signal for subsequent analysis.

8 Conclusions

Quasioptical techniques offer flexible solutions to design problems in the construction and use of high-field high-frequency EPR spectrometers. The design phase of the project is considerably aided by the techniques of Gaussian optics, which incorporates diffraction effects into a formalism that, within proper limits, is no more difficult to use than geometrical optics. The long wavelengths, typically of the order of millimeters, that are relevant for quasioptical systems in the near-millimeter band, combined with the high conductivity of most metals in this frequency regime means that fabrication of sophisticated, multi-element, low-loss quasioptical systems is within reach of most workshops, provided that due care is given to those tolerances, typically on the order of tenths of a millimeter, that influence the diffraction-limited performance of the optics. Furthermore, the inherently low-loss and high-power handling capabilities of quasioptical components make them strong candidates for use in high-power pulsed spectrometers.

Acknowledgements

Our understanding of the theoretical and practical aspects of quasioptical techniques has been greatly aided by interactions with a number of thoughtful and generous colleagues. We would like to thank Profs. Paul Goldsmith, David Budil, and Bryan Lynch, and Drs. Jeff Barnes, Richard Wylde and Graham Smith for invaluable conversations on a wide variety of topics. The services of the machine-shop facilities and staff of the Laboratory of Atomic and Solid State Physics, Cornell University, and the glass-shop of the Department of Chemistry and

Chemical Biology are also gratefully acknowledged. The research reviewed in this report was supported by grants from the NIH and NSF.

References

1. Lebedev Ya. in: Modern Pulsed and Continuous-Wave Electron Spin Resonance (Kevan L., Bowman M., eds.), pp. 365–404. New York: Wiley 1990.
2. Budil D.E., Earle K.A., Lynch W.B., Freed J.H. in: Advanced EPR: Applications in Biology and Biochemistry (Hoff A.J., ed.), pp. 307–340. Amsterdam: Elsevier 1989.
3. Earle K.A., Budil D.E., Freed J.H. in: Advances in Magnetic and Optical Resonance (Warren S.W., ed.), vol. 19, pp. 253–323. New York: Academic Press 1996.
4. Abragam A., Bleaney B.: Electron Paramagnetic Resonance of Transition Ions, pp. 125–132. New York: Dover 1986.
5. Eaton G.R., Eaton S.S., Rinard G.A. in: Spatially Resolved Magnetic Resonance: Methods, Materials, Medicine, Biology, Rheology, Geology, Ecology, Hardware (Blümer P., Blümich P., Botto R., Fukushima E., eds.), pp. 65–74. Weinheim: Wiley VCH 1998.
6. Galkin A.A., Grinberg O.Ya., Dubinskii A.A., Kabdin N.N., Krymov V.N., Kurochkin V.I., Lebedev Ya.S., Oranskii L.G., Shuvalov V.F.: Instrum. Exp. Tech. (Engl. Transl.) **20**, 1229 (1977)
7. Krymov V.N., Kurochkin V.I.: Projektirovaniye UHF chasty 2mm spectrometrov EPR (in Russian). Donetskii physico-technicheskii instituta Akademii Nauk Ukrainian SSR, Donetsk, 1985 (preprint).
8. Prisner T., Un S., Griffin R.G.: Isr. J. Chem. **32**, 357–363 (1992)
9. Allgeier J., Disselhorst J.A.J.M., Weber R.T., Wenckebach W.Th., Schmidt J. in: Modern Pulsed and Continuous-Wave Electron Spin Resonance (Kevan L., Bowman M., eds.), pp. 267–284. New York: Wiley 1990.
10. Haindl E., Möbius K., Oloff H.: Z. Naturforsch. A **40**, 169–172 (1985)
11. Lynch W.B., Earle K.A., Freed J.H.: Rev. Sci. Instrum. **59**, 1345–1351 (1988)
12. Earle K.A., Tipikin D.S., Freed J.H.: Rev. Sci. Instrum. **67**, 2502–2513 (1996)
13. Hassan A.K., Maniero A.-L., van Tol H., Brunel L.C. in: Magnetic Resonance and Related Phenomena (Ziessow D., Lubitz W., Lendzian F., eds.), pp. 121–122. Joint 29th Ampere - 13th ISMAR International Conference, Berlin August 2–7, 1998. Technische Universität Berlin: Berlin 1998.
14. Cardin J.T., Kolaczkowski S.V., Anderson J.R., Budil D.E.: Appl. Magn. Reson. **16**, 273–292 (1999)
15. Fuchs M., Weber S., Möbius K., Rohrer M., Prisner T. in: Magnetic Resonance and Related Phenomena (Ziessow D., Lubitz W., Lendzian F., eds.), pp. 119–120. Joint 29th Ampere - 13th ISMAR International Conference, Berlin August 2–7, 1998. Technische Universität Berlin: Berlin 1998.
16. Smith G.M., Lesurf J.C.G., Mitchell R.H., Riedi P.C.: Rev. Sci. Instrum. **69**, 3924–3937 (1998)
17. Goldsmith P.F.: Quasioptical Systems: Gaussian Beam Quasioptical Propagation and Applications. New York: IEEE Press 1998.
18. Misra S.K., Misiak L.E., Chand P.: Physica B **202**, 31–40 (1994)
19. Earle K.A., Budil D.E., Freed J.H.: J. Phys. Chem. **97**, 13289 (1993)
20. Barnes J.P., Freed J.H.: Rev. Sci. Instrum. **69**, 3022–3027 (1998)
21. Barnes J.P., Freed J.H.: Biophys. J. **75**, 2532–2546 (1998)
22. Earle K.A., Moscicki J.K., Polimeno A., Freed J.H.: J. Chem. Phys. **106**, 9996–10015 (1997)
23. Lynch W.B., Boorse R.S., Freed J.H.: J. Am. Chem. Soc. **115**, 10909–10915 (1993)
24. Shin D.-H., Dye J.L., Budil D.E., Earle K.A., Freed J.H.: J. Phys. Chem. **97**, 1213–1219 (1993)
25. Earle K.A., Budil D.E., Moscicki J.K., Ge M., Freed J.H.: Biophys. J. **66**, 1213–1221 (1994)
26. Barnes J.P., Freed J.H.: Rev. Sci. Instrum. **68**, 2838–2846 (1997)
27. Barnes J.P., Liang Z., Mchaourab H., Freed J.H., Hubbell W.: Biophys. J. (1999) in press.
28. Clarkson R.B., Smirnov A.I., Smirnova T.I., Kang H., Belford R.L., Earle K.A., Freed J.H.: Mol. Phys. **95** 1325–1332 (1998)

29. Poole C. Jr.: Electron Spin Resonance: A Comprehensive Treatise on Experimental Techniques, 2nd ed., pp. 381–458. New York: Dover 1983.
30. Doane J. in: Infrared and Millimeter Waves (Button K., ed.), vol. 13, pp. 123–170. New York: Wiley 1985.
31. General Atomics, "Corrugated Waveguides: Capabilities & Applications" Design Guide. New York: Dover 1995.
32. Jiang Y., Jing C., Peebles W.A., Bowers D.L., Doane J.L.: Rev. Sci. Instrum. **63**, 4672–4674 (1992)
33. Dragovan M.: Appl. Opt. **27**, 4076–4078 (1988)
34. Dionne G.F.: Int. J. Infrared Millimeter Waves **3**, 417–423 (1982)
35. Erickson N.R.: Appl. Opt. **18**, 956 (1979)
36. Costley A.E., Hursey K.H., Neill G.F., Ward J.M.: J. Opt. Soc. Am. **67**, 979–981 (1977)
37. Möbius K., Lubitz W., Plato M. in: Advanced EPR: Applications in Biology and Biochemistry (Hoff A., ed.), pp. 441–500. Amsterdam: Elsevier 1989.
38. Lesurf J.C.G.: Millimetre-Wave Optics, Devices, and Systems. Bristol: Adam Hilger 1990.

Authors' address: Prof. Dr. Jack H. Freed, Baker Laboratory of Chemistry and Chemical Biology, Cornell University, Ithaca, NY 14853-1301, USA